DEEP LEARNING-BASED USER CLUSTERING FOR MIMO-NOMA NETWORKS

Antoine Dejonghe[†]*, Carles Antón-Haro*[⋆]*, Xavier Mestre*[⋆]*, Leonardo Cardoso*[†] *and Claire Goursaud*[†]

[⋆]Centre Tecnològic de Telecomunicacions de Catalunya (CTTC/iCERCA)
Parc Mediterrani Tecnologia (PMT). Av Carl Friedrich Gauss 7, Bldg. B6, 08860 Castelldefels (SPAIN)
[†]Univ. Lyon, INSA Lyon, Inria, CITI
6, av. des Arts, 69621 Villeurbanne CEDEX (FRANCE)

ABSTRACT

The user clustering problem in an uplink MIMO Non-Orthogonal Multiple Access (NOMA) scheme is considered here. The receiver is assumed to operate in two sequential stages that employ Linear Minimum Mean Squared Error (LMMSE) receivers. At the first stage, the receiver is designed to recover the transmission from a cluster of selected users/nodes. The contribution of these users is then subtracted from the received signal and the remaining user transmissions are then linearly recovered. The determination of which users should be detected during the first stage is formulated as a deep learning based multiple classification problem. In order to guarantee that the selection is robust to fast fading, the input to the neural network is based on second order channel statistics. Furthermore, the training process is simplified by using a large system approximation of the resulting sum-rates. Simulation results indicate that the proposed deep learning-based solution is able to achieve a significant rate advantage with respect to other lazy approaches, such as fixed or random cluster assignments.

1. INTRODUCTION

The future increase in the Internet of Things (IoT) market requires the emergence of technical solutions that specifically address the challenges of this scenario [1]. Traffic generated by Machine Type Communications (MTC) devices is generally considered sporadic and may potentially entail a large volume of nodes that simultaneously communicate to a base station in grant-free manner. Furthermore, the simplicity of the MTC devices typically precludes any use of advanced power control and resource allocation strategies. In this context, the use of Non Orthogonal Multiple Access (NOMA) architectures [2] can provide significant advantages, since they do not really require advanced coordination among the different nodes and can potentially handle multiple users with very different received powers. Furthermore, NOMA architectures exhibit high spectral efficiency and can be easily combined with multi-antenna techniques.

The combination of MIMO and NOMA for the downlink has been deeply studied both for the downlink [3, 4] and for the uplink [5, 6]. In both cases, one of the most important problems is node pairing, namely grouping users in pairs so that they share a common resource, be it a frequency band or a spatial beam. In order to pair nodes, numerous methods have been proposed in the literature, where most of which specifically focus on the single antenna or the downlink scenario [5, 7, 13]. Our focus here is on the multi-antenna uplink scenario, where the number of studies is more scarce. Of particular interest is the work in [5], which considers the same scenario as the one in our paper, although with a slight modification in the user detection mechanism. Instead of considering successive interference cancellation, [5] considers joint decoding of the two paired user signals. This optimum decoding strategy is much more complex than conventional successive interference cancellation. Contrary to [5], we adopt a much simpler NOMA decoding strategy, whereby a selected subset of node transmissions are first linearly detected, individually decoded, and then subtracted from the received signal. Thereafter, the rest of the node transmissions are linearly detected from the "cleaned" version of the signal, and then individually decoded. We will assume a fixed power allocation and a slotted, grant-free, multiple access architecture.

For a total of N active nodes, there exist 2^N possible Clustering Solutions (CSs), which can lead to very different sum-rates. Here, we depart from other greedy/heuristic approaches attempting to e.g., minimize inter-cluster interference [19] or maximize channel gain disparity [20] in order to accomplish the task in a computationally-affordable manner. Instead, we design a clustering strategy based on Deep Learning (DL) tools, which generally offer a good trade-off between performance and computational complexity [11, 12]. DL has also been used in [14] to enhance the performance of grant-free NOMA, although in this work the goal was to design an end-to-end system rather than the user grouping stage. Another machine learning based approach for user clustering was pro-

THIS WORK IS SUPPORTED BY THE SPANISH GOVERNMENT THROUGH THE ARISTIDES PROJECT (RTI2018-099722-B-I00).

posed in [8], this time resorting to an unsupervised learning methodology based on K-means.

All the above learning methods, estimate the optimum NOMA user grouping based on *instantaneous* channel realizations which is computationally complex and expensive to implement. Here, instead, we propose a method using only the channel second order statistics (covariance matrices), which mostly depend on the geometry of the scenario and therefore remain constant over large periods of time.

2. SIGNAL AND SYSTEM MODEL

Consider the uplink of a multi-user SIMO system where a Base Station (BS) equipped with M antennas (Uniform Linear Array, ULA) serves N single-antenna active IoT devices (nodes). The received signal at the BS can be expressed as

$$\mathbf{y} = \mathbf{H}\mathbf{s} + \mathbf{n} \tag{1}$$

where $\mathbf{H} = [\mathbf{h}_1, \mathbf{h}_2, ..., \mathbf{h}_N] \in \mathbb{C}^{M\times N}$ is the channel matrix with $\mathbf{h}_n \in \mathbb{C}^M$ standing for the (column) channel vector associated to the n^{th} node; vector $\mathbf{s} \in \mathbb{C}^N$ accounts for the transmit signal, with its elements fulfilling $\mathbb{E}\left[\|s_i\|^2\right] = p_t; \forall i$, that is, transmit power is identical for all nodes and no power allocation or control mechanisms are in place. Finally, $\mathbf{n} \in \mathbb{C}^M$ denotes zero-mean i.i.d. additive white Gaussian noise of variance σ^2, namely, $\mathbf{n} \sim \mathcal{CN}(0, \sigma^2\mathbf{I}_M)$. Nodes operate at a central frequency f_c and follow a uniform spatial distribution in the served cell. We also assume that full Channel State Information (CSI) is available at the BS.

2.1. Channel model

Each column in the channel matrix $\mathbf{H} = [\mathbf{h}_1, \mathbf{h}_2, ..., \mathbf{h}_N]$ can be statistically modeled as $\mathbf{h}_n \sim \mathcal{CN}(0, \frac{1}{M}\mathbf{C}_n)$ where $\mathbf{C}_n \in \mathbb{C}^{M\times M}$ denotes the channel covariance matrix of the n-th node. We adopt a geometric channel model with L_p scattering paths that is widely used in the literature (see e.g., [22]). For large L_p, matrix $\mathbf{C}_n$ can thus be estimated as

$$\mathbf{C}_n = \frac{1}{\rho_n L_p}\sum_{l=1}^{L_p} |\alpha_{n,l}|^2 \mathbf{a}(\theta_{n,l})\mathbf{a}(\theta_{n,l})^H. \tag{2}$$

with ρ_n accounting for the path-loss *and* shadow-fading associated to the n-th node. Consequently, we have that $\rho_n = (1+ d_n^\eta)/10^{\frac{\beta_n}{10}}$, where d_n is the node-to-BS distance, η denotes the path-loss exponent (typically, $\eta \in [2, 6]$); and $\beta_n \sim \mathcal{N}(0, \sigma_\beta^2)$ is the spatially-uncorrelated shadow-fading coefficient, with σ_β^2 typically ranging from 6 dB (free-space propagation) to 10 dB (indoor environments) [16]. Further, the coefficient $\alpha_{n,l}$ of (2) is the complex gain (with $\mathbb{E}\left[|\alpha_{n,l}|^2\right] = 1$) of the l-th path; and $\theta_{n,l} \sim \mathcal{N}(\bar{\theta}_n, \sigma_\theta)$ denotes the angle-of-arrival (AoA) of the l-th path of node n, with $\bar{\theta}_n$ associated to the actual location of such node. Vector $\mathbf{a}(\theta_{n,l}) \in \mathbb{C}^{M\times 1}$ accounts for the antenna array response at the BS. For a ULA, it reads

$$\mathbf{a}\left(\theta_{n,l}\right) = \left[1, e^{-j\frac{2\pi}{\lambda}d\sin(\theta_{n,l})}, \ldots, e^{-j(M-1)\frac{2\pi}{\lambda}d\sin(\theta_{n,l})}\right]^T$$

where λ is the signal wavelength, and d is the distance between antenna elements. In the sequel, we assume $d = 0.5\lambda$. From all the above, the channel vector $\mathbf{h}_n$ can be computed as

$$\mathbf{h}_n = \left(\frac{1}{M}\mathbf{C}_n\right)^{1/2}\boldsymbol{\omega}_n \tag{3}$$

where $\boldsymbol{\omega}_n \sim \mathcal{CN}(0, \mathbf{I}_M)$. It is important to note that, in the above expression, the covariance matrix models the impact of path-loss and slow fading which, in turn, are associated to the physical location of the node. On the contrary, $\boldsymbol{\omega}_n$ models the effect of fast fading.

2.2. Multiple-access and decoding strategies

Let $\mathcal{N}$ denote the set of N active nodes in the system. We partition $\mathcal{N}$ into *two* disjoint subsets (clusters) $\mathcal{N}_1$ and $\mathcal{N}_2$ of cardinalities N_1 and N_2, and such that $N = N_1 + N_2$. The subset $\mathcal{N}_1$ is decoded first. After detection, the received signal associated to those nodes is reconstructed and its contribution removed from $\mathbf{y}$ (i.e., Successive Interference Cancellation, SIC, is performed) [15]. After this interference cancellation step, the nodes in the $\mathcal{N}_2$ subset are finally decoded. For a Linear Minimum Mean Square Error (LMMSE) receiver, the optimal beamformers $\mathbf{w}_n^{(1,2)} \in \mathbb{C}^M$ associated to an arbitrary node n in $\mathcal{N}_1$ or $\mathcal{N}_2$ read, respectively,

$$\mathbf{w}_n^{(1)} = (\mathbf{H}\mathbf{H}^H + \sigma^2\mathbf{I}_M)^{-1}\mathbf{h}_n \tag{4}$$
$$\mathbf{w}_n^{(2)} = (\mathbf{H}_{(\mathcal{N}_1)}\mathbf{H}_{(\mathcal{N}_1)}^H + \sigma^2\mathbf{I}_M)^{-1}\mathbf{h}_n \tag{5}$$

where matrix $\mathbf{H}_{(\mathcal{N}_1)}$ contains all the columns of $\mathbf{H}$ except for those corresponding to nodes from subset $\mathcal{N}_1$. Based on (4) and (5), one can easily prove that the instantaneous SINR for an arbitrary node in the first or second subsets read, respectively

$$\gamma_n^{(1)} = p_n\mathbf{h}_n^H(\mathbf{H}_{(n)}\mathbf{H}_{(n)}^H + \sigma^2\mathbf{I}_M)^{-1}\mathbf{h}_n \tag{6}$$
$$\gamma_n^{(2)} = p_n\mathbf{h}_n^H(\mathbf{H}_{(\mathcal{N}_1\cup\{n\})}\mathbf{H}_{(\mathcal{N}_1\cup\{n\})}^H + \sigma^2\mathbf{I}_M)^{-1}\mathbf{h}_n \tag{7}$$

Finally, the ergodic sum-rate *per node* R (i.e, normalized to the number of active nodes) can be expressed as:

$$R = \mathbb{E}_{\boldsymbol{\omega}_n}\left[\frac{1}{N}\sum_{n\in\mathcal{N}}\log_2(1 + \phi_n\gamma_n^{(1)} + \overline{\phi}_n\gamma_n^{(2)})\right] \tag{8}$$

where $\phi_n \in 0, 1$ is an indicator variable such that $\phi_n = 1$ if node n belongs to subset $\mathcal{N}_1$ and 0 otherwise; and $\overline{\phi}_n$ denotes the opposite of ϕ_n. Note also that (i) the expectation term in (8) is taken with respect to fast fading *only*; and (ii) the partitioning of nodes into subsets does not vary with fast fading.

3. ASYMPTOTIC SINRS AND ERGODIC SUM-RATE

Computing the ergodic sum-rate per node from the analytical expression (8) is computationally very intensive. To realize

that, it suffices to observe the matrix channel inversions of (6) and (7) and, also, the corresponding expected value that needs to be computed over the realizations of the fast fading (using, e.g. numerical integration or Monte-Carlo averaging). Interestingly enough, Random Matrix Theory (RMT) allows us to point out that, for large-enough values of N and M (i.e., the dimensions of matrix $\mathbf{H}$), the individual realizations of the SINRs almost surely converge to their average values [9]. More formally, we have $\gamma^{(i)} - \overline{\gamma}^{(i)} \rightarrow 0, i = 1, 2$ with probability one for a deterministic quantity $\overline{\gamma}^{(i)}$. Hence, the expectation in (8) can be dropped and the ergodic sum-rate per node becomes asymptotically equivalent to the quantity

$$\bar{R} = \frac{1}{N} \sum_{n \in \mathcal{K}} \log_2(1 + \phi_n \overline{\gamma}_n^{(1)} + \overline{\phi}_n \overline{\gamma}_n^{(2)}). \tag{9}$$

From [10] it follows that the asymptotic SINR for all the nodes belonging to the first subset can be computed in closed-form as

$$\overline{\gamma}_n^{(1)} = \frac{1}{M} tr \left[\mathbf{C}_n \left(\frac{1}{M} \sum_{\substack{j=1 \\ j \neq n}}^{N} \frac{\mathbf{C}_j}{(1 + \delta_j^n)} + \sigma^2 \mathbf{I}_M \right)^{-1} \right] \tag{10}$$

where $\{\delta_i\}_{i \in \mathcal{N} \setminus \{n\}}^n$ are the unique positive solutions to the system of $N - 1$ equations given by

$$\delta_i^n = \frac{1}{M} tr \left[\mathbf{C}_i \left(\frac{1}{M} \sum_{\substack{j=1 \\ j \neq n}}^{N} \frac{\mathbf{C}_j}{(1 + \delta_j^n)} + \sigma^2 \mathbf{I}_M \right)^{-1} \right] \tag{11}$$

with $i = 1, \ldots, N-1$. Similarly, for the nodes in subset two:

$$\overline{\gamma}_n^{(2)} = \frac{1}{M} tr \left[\mathbf{C}_n \left(\frac{1}{M} \sum_{j \in K_2 \setminus \{n\}} \frac{\mathbf{C}_j}{(1 + \zeta_j^n)} + \sigma^2 \mathbf{I}_M \right)^{-1} \right] \tag{12}$$

where $\{\zeta_i\}_{i \in \mathcal{N}_2 \setminus \{n\}}^n$ are, in turn, the unique positive solutions to the following system of $N_2 - 1$ equations:

$$\zeta_i^n = \frac{1}{M} tr \left[\mathbf{C}_i \left(\frac{1}{M} \sum_{j \in K_2 \setminus \{n\}} \frac{\mathbf{C}_j}{(1 + \zeta_j^n)} + \sigma^2 \mathbf{I}_M \right)^{-1} \right] \tag{13}$$

where $i = 1, \ldots, N_2 - 1$. As in [9], the systems of equations (11) and (13) can be efficiently solved via fixed point methods. Besides, it is important to note that in order to solve the aforementioned systems of equations, only the covariance matrices are needed as CSI. As discussed in Section 2.1, covariance matrices exclusively depend on the actual path-loss and slow fading (or, equivalently, on the physical location of nodes). In other words, the re-computation of $\overline{\gamma}^{(i)}$ is only needed whenever the *system* scenario changes and *not* for each realization of fast fading (i.e., at a slower rate).

Figure 1 illustrates the accuracy of the asymptotic approximation for the ergodic sum-rate per node for an increasing number of nodes (N) and BS antennas (M). This is accomplished via Monte Carlo simulations. For each tuple (M, N), results are averaged over system scenarios as well as all possible mappings of nodes onto subsets (clusters). As expected, for larger values of M and N, the asymptotic sum-rate per node converges to the analytic sum-rate. Specifically, for $M \geq 4$ and $N \geq 6$, the approximation becomes very accurate.

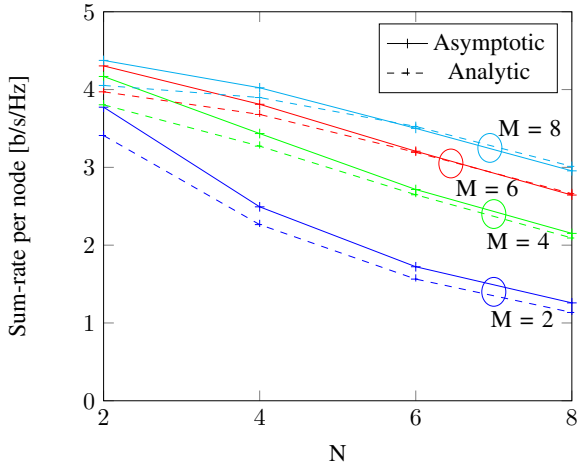

Fig. 1: Sum-rate per node for a varying number of nodes and antennas (SNR = 15 dB, $\sigma_\beta = 7$ dB, $\eta = 2$, $p_t = 0.1$ W, $L_p = 10$, $\sigma_\theta = 5°$).

4. PROBLEM FORMULATION

As discussed in previous sections, we aim at defining a partition of the set $\mathcal{N}$ of N nodes into two disjoint subsets (clusters) $\mathcal{N}_1$ and $\mathcal{N}_2$. Our goal is to maximize the ergodic sum-rate of a MIMO-NOMA system based on a LMMSE receiver and successive interference cancellation. In the sequel, we will refer to each of those possible node partitions as a *Clustering Solution* (CS). More formally, the problem can be formulated as follows:

$$\begin{aligned} \max_{\{\phi_1, \ldots \phi_N\}} \quad & \tfrac{1}{N} \textstyle\sum_{n \in \mathcal{N}} \log_2(1 + \phi_n \overline{\gamma}_n^{(1)} + \overline{\phi}_n \overline{\gamma}_n^{(2)}) \\ \text{s.t.} \quad & \phi_n \in \{0, 1\} \text{ for } n = 1 \ldots N \end{aligned} \tag{14}$$

where in the above expression we have already replaced the analytical sum-rate of (8) by its asymptotic approximation (9). From Section 3, the ergodic SINRs $\overline{\gamma}_n$ can be expressed as a function of the set of covariance matrices $\mathbf{C}_n \in \mathbb{C}^{M \times M}$ $n = 1 \ldots N$ (see equations (6) and (7)). In the sequel, we will thus consider the set of N covariance matrices $\{\mathbf{C}_n\}$ as a Sufficient Statistic (SS) to solve problem (14). This is in line with [21] where covariance matrices where used for learning-based *antenna selection*. Clearly, the number of inputs to the learning scheme N_s, which are typically stacked in a column vector (see next section), depends on the

number of elements in the SS. Since covariance matrices are Hermitian, half of the off-diagonal elements can be dropped and, thus, we have that $N_s = NM^2$.

5. DEEP LEARNING-BASED CLUSTERING

The task of selecting the optimal CS can be modeled as a supervised learning problem. Specifically it can be cast into a multi-class classification task where:

- The input for the p-th example is given by the sufficient statistics (i..e, the covariance matrices) associated to active nodes, namely, the row vector $\mathbf{t}_p = [t_{1,p}, \ldots, t_{N_s,p}] \in \mathbb{R}^{1\times N_s}$.
- The output is an index to the CS $c_p \in [1, \ldots, N_{\text{CS}}]$ yielding the highest sum-rate per node, with $N_{\text{CS}} = 2^N$ denoting the total number of Clustering Solutions.

5.1. Description of the training dataset

The training dataset comprises a total of P examples $\mathbf{t}_p$ stacked in a training matrix $\mathbf{T} = \left[\mathbf{t}_1^T, \ldots, \mathbf{t}_P^T\right]^T \in \mathbb{R}^{P\times N_s}$ and a class label vector $\mathbf{c} = [c_1, \ldots, c_P]^T \in \mathbb{N}^{P\times 1}$ that gathers the corresponding outputs. Its generation comprises the following steps:

1. Generation of the received signal for P realizations of system scenario (locations, path-loss, shadow-fading).
2. Computation of the covariance matrices $\mathbf{C}_n$ as a SS.
3. Computation of the sum-rates per node as per (10) and (12);
4. Letting the label of each example be the index of the clustering solution yielding the highest sum-rate per node, i.e., $\mathbf{c}_p \in \{1, \ldots, N_{\text{CS}}\}$.

To avoid significant bias in the training, features are normalized prior to their use by the learning scheme, namely, $t_{ij} \leftarrow (t_{ij} - E_i[t_{ij}]) \,/\, (\max_i [t_{ij}] - \min_i [t_{ij}])$. In addition, random under-sampling [18] is applied in order to prevent the formation of imbalanced training datasets (i.e., with over/under-represented classes). For cross-validation, 20% of the examples in the training dataset were set aside to generate the corresponding dataset.

5.2. Deep learning scheme

Feed-Forward deep Neural Networks (FFNN) can be regarded as universal function approximators. Our FFNN comprises L layers: (i) one input layer with N_s elements (see Section 4); (ii) one output layer with N_{CS} neurons (the total number of possible clustering solutions); and (iii) $L-2$ hidden layers with N_l neurons each. This FFNN defines a mapping $f(\mathbf{t}, \boldsymbol{\Psi}) : \mathbb{R}^{N_s} \mapsto \mathbb{R}^{N_{\text{CS}}}$ of an input vector $\mathbf{t}$ onto an output vector $\mathbf{r_L}$ through L iterative processing steps:

$$\mathbf{r}_l = f_l(\mathbf{r}_{l-1}, \boldsymbol{\psi}_l), l \in \{1, 2, 3, ..., L\} \tag{15}$$

where $f_l(\mathbf{r}_{l-1}, \boldsymbol{\psi}_l) : \mathbb{R}^{N_{l-1}} \mapsto \mathbb{R}^{N_l}$ is the mapping associated to the l^{th} layer. This mapping depends on the output from the previous layer and on the parameter set of that layer, $\boldsymbol{\psi}_l$, with $\boldsymbol{\Psi} = [\boldsymbol{\psi}_1, \boldsymbol{\psi}_2, ..., \boldsymbol{\psi}_L]$ denoting the set of all parameters in the model. The l-th layer is said to be dense if $f_l(\mathbf{r}_{l-1}, \boldsymbol{\psi}_l)$ is of the form

$$f_l(\mathbf{r}_{l-1}, \boldsymbol{\psi}_l) = \sigma(\mathbf{G}_l \mathbf{r}_{l-1} + \mathbf{b}_l) \tag{16}$$

where $\mathbf{G}_l \in \mathbb{R}^{N_l \times N_{l-1}}$ and $\mathbf{b}_l \in \mathbb{R}^{N_l}$ respectively denote a matrix of weights and a bias vector. In (16), $\sigma(.)$ is a non linear activation function. In this work, the activation function used for the hidden layers is the Rectified Linear Unit (ReLU) function. The activation function for the output layer is a softmax function so that each output computes the probability of such CS of yielding the highest sum-rate (an $\arg\max$ operator is applied to the set of outputs is order to make a final decision on the CS). Dropout is implemented after each hidden layer to prevent overfitting. During the training phase of the FFNN, the Adam optimizer is used to update the parameter set in each layer (i.e. $\boldsymbol{\psi}_l = [\mathbf{G}_l, \mathbf{b}_l]$). The goal is to minimize the categorical cross-entropy (i.e. maximize classification accuracy).

6. POWER-BASED HEURISTIC CLUSTERING

As an alternative to the learning-based approach of Section 5.2, here we propose a heuristic clustering scheme. It borrows inspiration from traditional clustering methods for power-domain NOMA (e.g., [17]) where, *prior to clustering*, nodes are sorted in a decreasing order of their channel gains. The method is low-complexity because it partitions the pre-sorted nodes into two clusters following a *fixed* pattern[1] for *all* system scenarios (unlike learning-based method which generate different CSs for different system scenarios). For example, the two strongest nodes are always mapped onto $\mathcal{N}_1$ (namely, $\phi_i = 0$ for $i = 1, 2$); whereas weakest ones are mapped onto $\mathcal{N}_2$ (i.e., $\phi_i = 1$ for $i > 2$). In the sequel, this clustering method will be referred to as PBHC (Power-Based Heuristic Clustering).

Similarly to [17], PBHC sorts nodes according to the trace of their channel covariance matrix $\{\mathbf{C}_n\}$ for each system scenario. To determine such fixed pattern, we must generate a large number of system scenarios (node locations, path-loss, slow-fading). After sorting nodes, we compute the sum-rate for each scenario and pattern. Finally, we find (via exhaustive search) the pattern that, on average, yields the highest sum-rate per node for the entire set of system scenarios. From now on, the same pattern will be used for every system scenario. The validity of this approach will be discussed next.

7. SIMULATION RESULTS

In this section, we consider a scenario with one BS equipped with $M = 4$ receive antennas, and $N = 6$ active nodes with

[1] For clarity, we use the term *pattern* when nodes are pre-sorted, and *clustering solution* otherwise.

identical transmit power ($p_t = 0.1$ W). The total number of clustering solutions is, thus, $N_{\text{CS}} = 2^N = 64$. As for channels, the path-loss exponent is $\eta = 2$ and for shadow fading we have that $\sigma_\beta = 7$ dB. The nodes are uniformly distributed in a rectangular area of 5×10 km, and for multi-path components ($L_p = 10$), the angular spread of their AoAs is $\sigma_\theta = 5°$. The carrier frequency is set to $f_c = 868$ MHz. The training dataset was generated by applying random undersampling on an imbalanced dataset of 90.000 examples. The size of the balanced dataset turned out to be different for each SNR (e.g., $P = 55.000$ examples at SNR=5 dB). On the contrary, we let $P_{\text{test}} = 10.000$ examples for the test dataset in all cases. Note also that the FFNN only needs to be re-trained when the system scenario changes (e.g., when the number of user varies). Otherwise, the spatial information embedded in the covariance matrix (e.g., node locations, path-loss, slow fading) suffices to perform user clustering with the previously-trained FFNN. As for FFNNs, the number of layers and neurons in the hidden layers is $L = 5$ and $N_l = 2^{(N+1)}$, respectively; with a dropout rate of 20% which sufficed to prevent overfitting. The initial learning rate is set to 10^{-3}, and the batch size is 32. In addition to PBHC, we also include two benchmarks (i) *random* clustering, with uniform distribution; and (ii) *optimal* clustering via exhaustive search.

The solid lines of Figure 2 (top) depict the total sum-rate of each CS for three specific realizations of the system scenario (each denoted by a different color) sorted in a decreasing order of sum-rates. Interestingly, the sum-rate span (difference between the best and worst CSs) is on the order of 15 b/s/Hz. This substantiates the need for efficient clustering algorithms. Dashed lines indicate the achievable sum-rate via FFNN. In one scenario (green curves), FFNN fails to select the optimal CS[2]. Nevertheless, the penalty in terms of sum-rate is rather limited (1 b/s/Hz, approximately). Complementarily, Fig. 2 (bottom) illustrates the Cumulative Density Function (CDF) of the sorted CSs. Despite that FFNN only succeeds in selecting the optimal CS in 35% of the system scenarios, it still manages to find one out of the 8 best CSs for 80% of the cases (marginal sum-rate loss). This is in stark contrast with PBHC where, for a cumulative probability of 80%, this requirement should be relaxed to one out of the 32 best CSs (which entails a larger sum-rate penalty). Note, however, that the computational complexity of PBHC is substantially lower, since the optimal clustering pattern is hold fixed (i.e., no need to re-compute covariance matrices, solve a system of equations or perform inference whenever e.g., users move).

Next, we investigate sum-rate performance. In Fig. 3, we depict the Cumulative density function (CDF) of the sum-rate achievable with the various clustering methods. It is important to note that the CDF associated to FFNN-based clustering is very close to that of the optimal clustering. On the contrary, the gap for PBHC and random clustering is much wider. Finally, in Fig. 4 we show the sum-rate performance

[2]This is due to the high number of classes and to the fact that decisions regions for this problem are rather complex (e.g., not connected, overlapping).

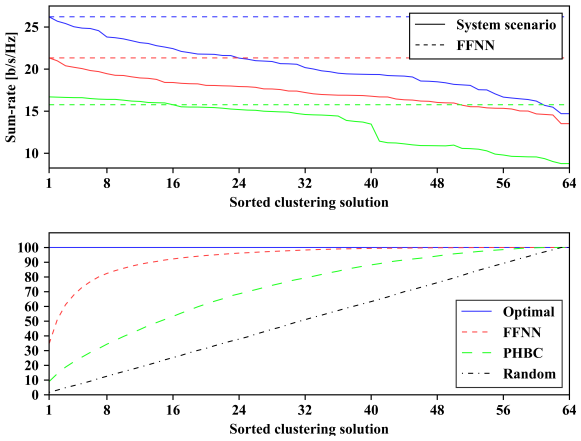

Fig. 2: Sum-rate of CSs for three realizations of the system scenario, top; and CDF of sorted CSs, bottom; SNR = 15 dB.

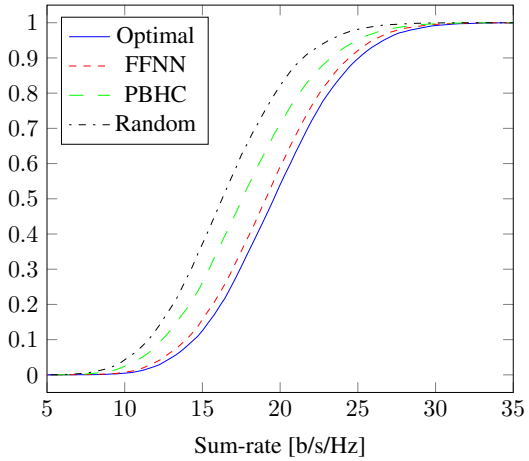

Fig. 3: CDF of the sum-rate (SNR = 15 dB).

of the learning-based clustering method along with that of the various benchmarks. Interestingly, the sum-rate of the FFNN approach is very close to that of optimal clustering via exhaustive search (loss below 1 b/s/Hz). This is due to the fact that, with high probability, FFNN is able to identify one of the (very few) CSs with the highest sum-rate. For large SNR, it provides a sum-rate gain of 30% with respect to random clustering, and 19% with respect to the heuristic PBHC approach.

8. CONCLUSIONS

In this work we have investigated the applicability of deep-learning to node clustering in MIMO-NOMA systems. Specifically, we have resorted to a feed-forward neural network to partition nodes into two disjoint clusters and, by doing so,

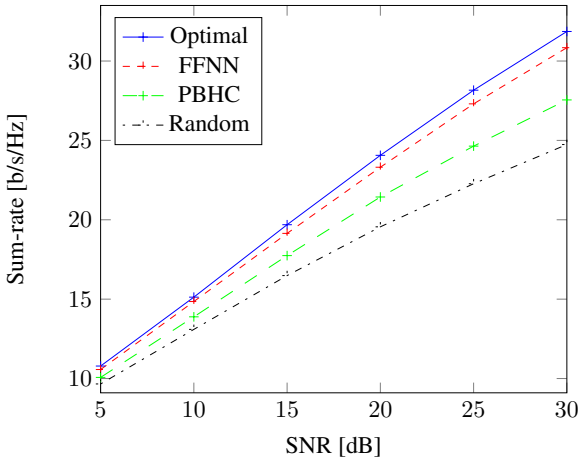

Fig. 4: Sum-rate vs SNR for each clustering method.

maximize the resulting ergodic sum-rate. In order to build the training datasets and efficiently train the learning system, we have derived analytical expressions for the asymptotic SINRs and ergodic sum-rates based on random matrix theory tools. Computer simulation results revealed that the sum-rate performance of the proposed FFNN scheme is very close to optimal, and that FFNN clearly outperforms PBHC which exhibits a lower computational complexity.

9. REFERENCES

[1] L. Horwitz, "The future of IoT miniguide: The burgeoning IoT market continues", Cisco, 2019.

[2] Y. Saito, Y. Kishiyama, A. Benjebbour, T. Nakamura, A. Li and K. Higuchi, "Non-Orthogonal Multiple Access (NOMA) for Cellular Future Radio Access," 2013 IEEE 77th Vehicular Technology Conf. (VTC Spring), 2013.

[3] Z. Ding, F. Adachi and H. V. Poor, "The Application of MIMO to Non-Orthogonal Multiple Access," IEEE Transactions on Wireless Communications, vol. 15, no. 1, pp. 537-552, Jan. 2016.

[4] Y. Huang, C. Zhang, J. Wang, Y. Jing, L. Yang and X. You, "Signal Processing for MIMO-NOMA: Present and Future Challenges," IEEE Wireless Communications, vol. 25, no. 2, pp. 32-38, April 2018.

[5] M. A. Sedaghat and R. R. Müller, "On User Pairing in Uplink NOMA," IEEE Trans. on Wireless Communications, vol. 17, no. 5, pp. 3474-3486, May 2018.

[6] Z. Ding, R. Schober and H. V. Poor, "A General MIMO Framework for NOMA Downlink and Uplink Transmission Based on Signal Alignment," in IEEE Trans. Wireless Comms, vol 15, no 6, pp. 4438-4454, June 2016.

[7] M. Al-Imari, P. Xiao, M. A. Imran and R. Tafazolli, "Uplink non-orthogonal multiple access for 5G wireless networks," 2014 11th Int'l Symposium on Wireless Comms. Systems (ISWCS), Barcelona, 2014, pp. 781-785.

[8] J. Cui, Z. Ding, P. Fan and N. Al-Dhahir, "Unsupervised Machine Learning-Based User Clustering in mmWave-NOMA Systems," IEEE Trans. on Wireless Comms., vol. 17, no. 11, pp. 7425-7440, Nov. 2018.

[9] J. Hoydis, S. ten Brink and M. Debbah, "Massive MIMO in the UL/DL of Cellular Networks: How Many Antennas Do We Need?," IEEE Journal on Selected Areas in Comms., vol. 31, no. 2, pp. 160-171, Feb. 2013.

[10] S. Wagner, R. Couillet, M. Debbah and D. T. M. Slock, "Large System Analysis of Linear Precoding in Correlated MISO Broadcast Channels Under Limited Feedback," IEEE Transactions on Information Theory, vol. 58, no. 7, pp. 4509-4537, July 2012.

[11] Y. Lecun, Yann, Y. Bengio, G. Hinton, "Deep learning", Nature, vol. 521, no 7553, pp. 436-444, 2015.

[12] E. Min, X. Guo, Q. Liu, G. Zhang, J. Cui and J. Long, "A Survey of Clustering With Deep Learning: From the Perspective of Network Architecture," IEEE Access, vol. 6, pp. 39501-39514, 2018.

[13] Z. Mlika, S. Cherkaoui, "Massive Access in Beyond 5G IoT Networks with NOMA: NP-hardness, Competitiveness and Learning", preprint arXiv:2002.07957, 2020.

[14] N. YE, X. Li, H. Yu *et al.* "Deep learning aided grant-free NOMA toward reliable low-latency access in tactile Internet of Things", IEEE Trans. on Industrial Informatics, 2019, vol. 15, no 5, p. 2995-3005.

[15] A.J. Viterbi. Very low rate convolutional codes for maximum theoretical performance of spread-spectrum multiple-access channels. IEEE Journal on Selected Areas in Comms., 1990, vol. 8, no 4, p. 641-649.

[16] B. Sklar, "Rayleigh fading channels in mobile digital communication systems. Characterization," in IEEE Comms. Magazine, vol 35, no 7, pp. 90-100, July 1997.

[17] M. S. Ali, H. Tabassum and E. Hossain, "Dynamic User Clustering and Power Allocation for Uplink and Downlink Non-Orthogonal Multiple Access (NOMA) Systems," IEEE Access, vol. 4, pp. 6325-6343, 2016.

[18] S. Kotsiantis, D. Kanellopoulos, P. Pintelas, "Handling imbalanced datasets: A review", GESTS International Transactions on Computer Science and Engineering, 2006, vol. 30, no 1, p. 25-36.

[19] X. Hu *et al.*, "Cluster Grouping and Power Control For Angle-Domain MmWave MIMO NOMA Systems",IEEE Journal of Selected Topics in Signal Processing, vol. 13, no. 5, pp. 1167-1180, Sept. 2019.

[20] A. Celik *et al.*, "Distributed User Clustering and Resource Allocation for Imperfect NOMA in Heterogeneous Networks", IEEE Trans. on Comms., vol. 67, no. 10, pp. 7211-7227, Oct. 2019.

[21] M. Ibrahim, *et al.*, "Learning-based antenna selection for multicasting", IEEE Int'l Workshop on Signal Proc. Advances in Wireless Comms. (SPAWC), 2018.

[22] S. Park, A. Ali, N. González-Prelcic and R. W. Heath, "Spatial Covariance Estimation for the Hybrid Architecture at a Base Station: a Tensor-decomposition.based Approach," IEEE GlobalSIP Conference, Anaheim, 2018.